Atmos. Chem. Phys. Discuss., 14, 3733–3775, 2014
www.atmos-chem-phys-discuss.net/14/3733/2014/
doi:10.5194/acpd-14-3733-2014
© Author(s) 2014. CC Attribution 3.0 License.

Atmospheric Chemistry and Physics Discussions

This discussion paper is/has been under review for the journal Atmospheric Chemistry and Physics (ACP). Please refer to the corresponding final paper in ACP if available.

Definition of the energy norm induced metric and its application on the atmosphere

F. Wan[1,2] **and T.-Y. Koh**[1,2]

[1]School of Physical and Mathematical Sciences, Nanyang Technological University, Singapore
[2]Earth Observatory of Singapore, Nanyang Technological University, Singapore

Received: 6 January 2014 – Accepted: 29 January 2014 – Published: 11 February 2014

Correspondence to: T.-Y. Koh (kohty@ntu.edu.sg)

Published by Copernicus Publications on behalf of the European Geosciences Union.



Abstract

We suggest that some energy metrics are based on linearization and hence it may not be appropriate to apply these metrics when two states are far apart such as encountered in the real atmosphere. A new approach of defining the energy metric is proposed which is based on rigorous mathematical principles and can be applied to both linear and nonlinear models. The new energy norm induced metric is derived for atmospheric models of various levels of sophistication: the 2-D barotropic model, the shallow-water model, the 3-D compressible dry model in different vertical coordinates. Numerical calculations of the new energy metric are illustrated with analytic dynamical systems as well as with global reanalysis data. The differences from other expressions of the energy metric in the literature are discussed and possible shortcomings in certain expressions are explained in the context of the new expression.

1 Introduction

In the study of weather predictability, the sensitivity of numerical models to the initial conditions is centre-stage. It has been demonstrated in Lorenz's (1963) pioneer work that slightly different initial states diverge exponentially over time. Thus, theoretical predictability is often measured by the exponential growth rates of small initial errors (Lorenz, 1965). Predictability in practice also entails the quality of observations and the fidelity of models. We are addressing only the theoretical predictability intrinsic to the dynamics of the system (Yoden, 1987). The fundamental concept of a metric is implicit to the definition of error growth, i.e. the distance between two states in the phase space.

Theoretically, one can adopt any kind of norm to measure the distance between two points in the phase space as long as the expression satisfies the definition of a norm. But some of them may be interpreted with physical meanings while others may not. In one dimensional space for example, when the geopotential height is the only variable

ACPD
14, 3733–3775, 2014



considered, the metric may be defined simply as the absolute value of the difference (Ding and Li, 2007). In multidimensional space, there are various ways of defining a metric (Lorenz, 1969; Molteni and Palmer, 1993; Mu and Duan, 2003; Mu et al., 2003). The states of the atmosphere are multidimensional vectors, and hence a norm needs to combine the variables in each dimension for a single measure.

The total energy norm is the most commonly used norm to measure the distance between two states of the atmosphere. The expressions of the total energy norm are varied in literature. Some used expressions similar to the wave energy (Bannon, 1995; Zou et al., 1997; Kim et al., 2011), while others used quadratic expressions (Buizza et al., 1993; Zhang et al., 2003; Leutbecher and Palmer, 2008; Rivière et al., 2009). Palmer et al. (1998) summarized and compared a number of metrics based on enstrophy, total energy and kinetic energy, which are defined by inner product.

Many different forms of total energy norms are based on a conserved quantity of the governing equations linearized about a reference state at rest with homogenous temperature $T_\circ$ and surface pressure $p_\circ$ in the case of no surface topography. From Talagrand (1981), the quadratic conserved total energy of the perturbed flow over a horizontal domain A is

$$E = \frac{1}{2}\int_A \int_0^{p_\circ} \left(u^2 + v^2 + \frac{c_p}{T_\circ}T^2\right) \mathrm{d}p\mathrm{d}A + \frac{1}{2}\int_A \frac{RT_\circ}{p_\circ} p_\mathrm{s}^2 \mathrm{d}A, \quad (1)$$

where c_p and R are specific heat at constant pressure and specific gas constant of dry air. The state variables u, v, T, and p_s are the perturbed zonal and meridional wind velocities, temperature and surface pressure respectively.

The total energy norm defined in Eq. (1) was originally developed to study the convergence of data assimilation in Talagrand (1981). It is used later by many authors (Ehrendorfer and Errico, 1995; Errico, 2000; Qin and Mu, 2012) to measure the growing components of a flow. In such cases, the constant $T_\circ$ in Eq. (1) has lost its original meaning as a reference state due to wide departure of realistic states from uniform temperature and should be replaced by more realistic forms of T (Ehrendorfer and Errico,

ACPD
14, 3733–3775, 2014



1995). The limitation of Talagrand's energy metric is that it is based on linearization, which means all perturbed variables are assumed to be small in Eq. (1). However, this assumption is not guaranteed when two states are far away from each other and should be tested in applications.

This paper aims to develop a new metric based on energy that overcomes the limitations of linearization and unrealistic simple reference states. The organization of the paper is as follows. Section 2 develops the new metric in the 2-D barotropic model and the shallow-water model. Section 3 describes the new metric in the 3-D compressible model with different vertical coordinates. In Sects. 4 to 6, numerical calculations of the new metric for the three models are illustrated with analytic dynamical systems and reanalysis data. The conclusions are summarized in the final section.

2 Simple fluid systems

A norm on S can be any function $\|\cdot\| : S \rightarrow [0, +\infty)$ which satisfies the following properties (Davidson and Donsig, 2010): positive definiteness, homogeneity and triangle inequality. Although given the flexibility of defining the norm, some of the norms may be interpreted with physical meanings while others may not when a physical interpretation is given to the vector space. When it comes to atmospheric dynamical systems whose physical states can be regarded as a vector space, a very natural and obvious candidate for the norm is energy, which is essentially a conserved quantity of the unforced, frictionless insulated flow. The uniqueness and importance of energy is the conservative property so that any change in energy means there is an external energy flux in and/or out of the system.

In a normed vector space, the metric between two vectors can be defined as norm of the difference between the two vectors, which is called norm induced metric. A metric must satisfies the following properties: positive definiteness, symmetry and triangle inequality (Davidson and Donsig, 2010). We have the following hierarchy (Davidson

ACPD
14, 3733–3775, 2014



and Donsig, 2010)

$\{\text{metric space}\} \supsetneq \{\text{normed space}\} \supsetneq \{\text{inner product space}\}$.

When an inner product is defined for a vector space, the inner product of the difference between two vectors with itself yields the square of the norm-induced metric. In the literature, both the norm (Buizza et al., 1993; Ehrendorfer and Errico, 1995; Leutbecher and Palmer, 2008) and the inner product (Palmer et al., 1998) have been used to define metric.

In this section, the energy norm and the norm induced metric are defined and verified on the phase space of two simple atmospheric systems namely the 2-D barotropic model and the shallow-water model as a first illustration. The two models are assumed to cover a horizontal domain A with periodic lateral boundary conditions.

2.1 2-D barotropic model

For a 2-D barotropic model in Cartesian coordinates x and y, the kinetic energy,

$$E = \frac{\rho_\circ}{2} \int_A \left(u^2 + v^2\right) \mathrm{d}A, \tag{2}$$

is conserved, where $\boldsymbol{u} = (u, v)$ is the horizontal velocity vector, $\rho_\circ$ is the density. The barotropic flow is fully described by the phase vector $\boldsymbol{x} = (u, v)$, and all the possible states form the phase space. It is easy to verify that energy could be used to defined a norm such that $\|\boldsymbol{x}\|^2 = E$, which is actually the Euclidean norm on the phase space.

Let $\boldsymbol{x}_1$ and $\boldsymbol{x}_2$ be two vectors in the phase space, then the norm induced metric is defined by

$$\|\boldsymbol{x}_1 - \boldsymbol{x}_2\|^2 = \frac{\rho_\circ}{2} \int_A \left((u_1 - u_2)^2 + (v_1 - v_2)^2\right) \mathrm{d}A, \tag{3}$$

ACPD
14, 3733–3775, 2014



which is similar to the error kinetic energy defined by (Lorenz, 1969).

Actually the square of the norm induced metric $\|\boldsymbol{x}_1 - \boldsymbol{x}_2\|^2$ also satisfies the definition of a metric, which is called separation metric hereafter. The separation metric is used as the metric to measure the distance between two states in this work.

2.2 Shallow-water model

For shallow-water model, the sum of kinetic and geopotential energy,

$$E = \frac{1}{2}\int_A (h\boldsymbol{u}^2 + gh^2)\mathrm{d}A, \tag{4}$$

is conserved (Vallis, 2006), where h is the thickness of the flow, g is the gravitational acceleration, and the other symbols have the same meaning as in the barotropic model. Before making use of this energy expression as a norm, the subtle question is how the phase vector should be defined.

The easiest way of defining the phase space is adding another dimension to the phase space of the barotropic model, which results in a three-dimensional phase vector (u, v, h) and use the square root of Eq. (4) as the norm. However, since Eq. (4) is not quadratic, it is positive definite for a single state but not for the difference vector between two states. So we cannot use Eq. (5) to define a metric for this phase space.

The phase vector is defined instead as $(\sqrt{h}u, hv, h)$ so that the energy is the Euclidean norm in this phase space. Let $\boldsymbol{x}_1 = (\sqrt{h_1}u_1, \sqrt{h_1}v_1, h_1)$ and $\boldsymbol{x}_2 = (\sqrt{h_2}u_2, \sqrt{h_2}v_2, h_2)$ be two phase vectors, then the separation metric (or the square of the norm induced metric) is given by

$$\|\boldsymbol{x}_1 - \boldsymbol{x}_2\|^2 = \frac{1}{2}\int_A \left((\delta\sqrt{h}\boldsymbol{u})^2 + g(\delta h)^2\right)\mathrm{d}A, \tag{5}$$

where $\delta\boldsymbol{x} = \boldsymbol{x}_1 - \boldsymbol{x}_2$.

ACPD
14, 3733–3775, 2014



2.3 Linearization of separation

Let the norm be $E = f(a,b) + g(a,b)$, where f and g are positive definite functions of variables a and b, so that E is the Euclidean norm of vector space $\{\boldsymbol{x} \in S | \boldsymbol{x} = (\sqrt{f}, \sqrt{g})\}$. If variables a and b are observed and recorded in practice, it is more convenient to transform $(\sqrt{f}, \sqrt{g})$ coordinates to the more conventional (a,b) coordinates. Although the relation between the two coordinate systems may involve nonlinear transformations, the increments $(\delta\sqrt{f}, \delta\sqrt{g})$ can be approximated by the linear combinations of $(\delta a, \delta b)$ assuming the increments are small (Fleisch, 2011). One example is the transformation from Cartesian (x,y,z) to spherical polar (λ,ϕ,r) coordinates where λ is longitude, ϕ is latitude and r is the distance from origin (Fleisch, 2011).

The norm induced metric in $(\sqrt{f}, \sqrt{g})$ coordinates is given by

$$\|\boldsymbol{x}_1 - \boldsymbol{x}_2\|^2 = (\delta\sqrt{f}, \delta\sqrt{g})(\delta\sqrt{f}, \delta\sqrt{g})^{\mathrm{T}}. \tag{6}$$

Using total increment theorem, Eq. (6) can be approximated in the tangent space $\{\delta\boldsymbol{x} = (\delta a, \delta b)\}$ by

$$\|\boldsymbol{x}_1 - \boldsymbol{x}_2\|^2 \approx (\delta a, \delta b)\mathbf{G}(\delta a, \delta b)^{\mathrm{T}}, \tag{7}$$

where the metric tensor

$$\mathbf{G} = \frac{1}{4}\begin{pmatrix} f_a^2/f + g_a^2/g & f_a f_b/f + g_a g_b/g \\ f_a f_b/f + g_a g_b/g & f_b^2/f + g_b^2/g \end{pmatrix}, \tag{8}$$

where the subscripts denote derivatives with respect to that variable. Notice that when $f = a^2$ and $g = b^2$, the metric tensor is simply the identity matrix and Eq. (7) reproduces the Euclidean norm.

In the shallow-water model, we may transform $(\sqrt{h}u, \sqrt{h}v, h)$ coordinates to the more familiar (u,v,h) coordinates. If two vectors $\boldsymbol{x}_1$ and $\boldsymbol{x}_2$ are close to each other, the total

ACPD
14, 3733–3775, 2014



increment $\delta\sqrt{h}u$ can be linearized about a reference state which could be either one of the two vectors. Hence, Eq. (5) can be rewritten as

$$\|\boldsymbol{x}_1 - \boldsymbol{x}_2\|^2 \approx \frac{1}{2}\int_A (\delta u, \delta v, \delta h) \begin{pmatrix} h & 0 & u/2 \\ 0 & h & v/2 \\ u/2 & v/2 & (u^2+v^2)/4h + g \end{pmatrix} \begin{pmatrix} \delta u \\ \delta v \\ \delta h \end{pmatrix} \mathrm{d}A, \tag{9}$$

which is non-Euclidean as the metric tensor matrix is not diagonal.

3 Dry compressible atmosphere

In this section, the definition of the separation metric is extended using the same methodology to fully compressible equations of dry, adiabatic and inviscid atmosphere in different vertical coordinates. The domain A is assumed to be enclosed or periodic.

3.1 Pressure coordinate

In pressure coordinate, it can be proved that the following quantity is conserved (Trenberth, 1997)

$$E = \frac{1}{g}\int_A \int_0^{p_\mathrm{H}} \left(\frac{1}{2}\boldsymbol{u}^2 + c_p T + \Phi_\mathrm{H}\right) \mathrm{d}p\mathrm{d}A, \tag{10}$$

where T is the temperature, Φ_H is the surface geopotential, p_H is the surface pressure, R is the gas constant for dry air, c_p is the specific heat of dry air at constant pressure, and the other symbols follow the same notation as Sect. 2. The energy Eq. (10) is not quadratic as p_H appears as a variable in the upper limit of integration, which means Eq. (10) cannot be used directly to define metric.

ACPD
14, 3733–3775, 2014



Notice that for a given location (x,y), the surface pressure anomaly of O(10 mb) is usually small compared to its climatology value. A reference pressure

$$p_r(x,y) = [p_H(x,y,t)]_t - 100\,\text{mb}, \tag{11}$$

where square bracket $[\cdot]_t$ denotes mean over time, could be chosen (see Appendix A for the reason of such choice) such that the vertical integration in Eq. (10) could be separated into a main body $[0, p_r]$ and a boundary layer $[p_r, p_H]$. In the boundary layer, the kinetic energy $1/2\boldsymbol{u}^2$ is always much less than $c_pT + \Phi_H$ and the vertical mean temperature is assumed to be rather stable temporally hence can be approximated by the boundary-layer climatology defined by

$$T_r(x,y) = \left[\int_{p_r}^{p_H} T\,\mathrm{d}p/(p_H - p_r)\right]_t. \tag{12}$$

So Eq. (10) can be approximated by

$$E \approx \frac{1}{g}\int_A\int_0^{p_r}\left(\frac{1}{2}\boldsymbol{u}^2 + c_pT + \Phi_H\right)\mathrm{d}p\mathrm{d}A + \frac{1}{g}\int_A (c_pT_r + \Phi_H)(p_H - p_r)\mathrm{d}A. \tag{13}$$

The approximated energy expression Eq. (13) is used to define the norm with phase vector defined as $\boldsymbol{x} = (u, v, \sqrt{T}, \sqrt{p_H - p_r})$ since Φ_H and T_r are time-independent. Let $\boldsymbol{x}_1$ and $\boldsymbol{x}_2$ be two vectors in the phase space, then the separation metric of compressible flow in pressure coordinate is given by

$$\|\boldsymbol{x}_1 - \boldsymbol{x}_2\|^2 = \frac{1}{g}\int_A\int_0^{p_r}\frac{1}{2}(\delta\boldsymbol{u})^2\mathrm{d}p\mathrm{d}A + \frac{1}{g}\int_A\int_0^{p_r} c_p(\delta\sqrt{T})^2\mathrm{d}p\mathrm{d}A + \frac{1}{g}\int_A (c_pT_r + \Phi_H)(\delta\sqrt{p_H - p_r})^2\mathrm{d}A, \tag{14}$$

ACPD
14, 3733–3775, 2014



where the three integrals are called kinetic, enthalpy and surface pressure components of separation respectively. The surface pressure component is mainly contributed by the enthalpy fluctuations due to mass fluctuations in the boundary layer.

Equation (14) could be approximated in terms of perturbations of the more conventional variables u, v, T and p_H as below

$$\|\boldsymbol{x}_1 - \boldsymbol{x}_2\|^2 \approx \frac{1}{g}\int_A \int_0^{p_r} \left(\frac{1}{2}(\delta \boldsymbol{u})^2 + c_p \frac{(\delta T)^2}{4T}\right) \mathrm{d}p\mathrm{d}A + \frac{1}{g}\int_A (c_p T_r + \Phi_H)\frac{(\delta p_H)^2}{4(p_H - p_r)}\mathrm{d}A. \quad (15)$$

The approximation of the first integral in Eq. (14) requires the temperature difference to be much smaller than temperature itself and the approximation of the second integral is always appropriate as $\delta p_H/(p_H - p_r)/4 \ll 1$.

The linearized separation metric Eq. (15) is different from the total energy norm Eq. (1) in the coefficients of temperature difference $(\delta T)^2$ and surface pressure difference $(\delta p_H)^2$. For the coefficient of temperature difference, our linearization is about a spatially varying temperature, and there is a factor 2 present.

3.2 Isentropic coordinate

In isentropic coordinate, the following quantity is conserved (Trenberth, 1997; Staniforth and Wood, 2003)

$$E = \int_A \int_{\theta_H}^{\infty} \left(\frac{1}{2}\sigma \boldsymbol{u}^2 + c_p \sigma T + \sigma \Phi_H\right) \mathrm{d}\theta \mathrm{d}A, \quad (16)$$

where $\sigma = -g^{-1}\partial p/\partial\theta$ is the isentropic coordinate density, θ is potential temperature, and the other symbols follow the same notation as previous sections. Similar to the case of pressure coordinate, we define an appropriate reference potential temperature $\theta_r(x,y)$ to separate the main body and the boundary layer. Using the boundary-layer climatology to approximate values between surface and θ_r and neglecting the

ACPD
14, 3733–3775, 2014



boundary-layer kinetic energy, we have

$$E \approx \int_A \int_{\theta_r}^{\infty} \left(\frac{1}{2}\sigma \boldsymbol{u}^2 + c_p \sigma T + \sigma \Phi_H \right) \mathrm{d}\theta \mathrm{d}A + \int_A \sigma_r (c_p T_r + \Phi_H)(\theta_r - \theta_H) \mathrm{d}A, \tag{17}$$

where

$$\sigma_r = \left[\int_{\theta_H}^{\theta_r} \sigma \mathrm{d}\theta / (\theta_r - \theta_H) \right]_t, \text{ and } T_r = \left[\int_{\theta_H}^{\theta_r} \sigma T \mathrm{d}\theta / (\sigma_r (\theta_r - \theta_H)) \right]_t. \tag{18}$$

Therefore we define the phase vector as $\boldsymbol{x} = (\sqrt{\sigma}u, \sqrt{\sigma}v, \sqrt{\sigma T}, \sqrt{\sigma}, \sqrt{\theta_r - \theta_H})$ and the separation metric in isentropic coordinate based on Eq. (17) is given by

$$\|\boldsymbol{x}_1 - \boldsymbol{x}_2\|^2 = \int_A \int_{\theta_r}^{\infty} \left(\frac{1}{2}(\delta\sqrt{\sigma}\boldsymbol{u})^2 + c_p(\delta\sqrt{\sigma T})^2 + \Phi_H(\delta\sqrt{\sigma})^2 \right) \mathrm{d}\theta \mathrm{d}A$$
$$+ \int_A \sigma_r (c_p T_r + \Phi_H)(\delta\sqrt{\theta_r - \theta_H})^2 \mathrm{d}A. \tag{19}$$

The second integral in Eq. (19) reflects enthalpy changes due to mass fluctuations in the boundary layer, which is the same idea as in pressure coordinate. The phase vector in isentropic coordinate has both the density dimension $\sqrt{\sigma}$ and the boundary-layer thickness dimension $\sqrt{\theta_r - \theta_H}$. The linearized version of Eq. (19) is given by

$$\|\boldsymbol{x}_1 - \boldsymbol{x}_2\|^2 \approx \int_A \int_{\theta_r}^{\infty} \left[\frac{1}{2} \left(\sigma(\delta\boldsymbol{u})^2 + \boldsymbol{u} \cdot \delta\boldsymbol{u}\delta\sigma + \frac{\boldsymbol{u}^2}{4\sigma}(\delta\sigma)^2 \right) \right.$$

ACPD
14, 3733–3775, 2014



$$+c_p\left(\frac{\sigma}{4T}(\delta T)^2+\frac{\delta\sigma\delta T}{2}+\frac{T}{4\sigma}(\delta\sigma)^2\right)+\Phi_{\mathrm{H}}\frac{(\delta\sigma)^2}{4\sigma}\Bigg]\mathrm{d}\theta\mathrm{d}A$$

$$+\int_A\sigma_{\mathrm{r}}(c_pT_{\mathrm{r}}+\Phi_{\mathrm{H}})\frac{(\delta\theta_{\mathrm{H}})^2}{4(\theta_{\mathrm{r}}-\theta_{\mathrm{H}})}\mathrm{d}A. \tag{20}$$

3.3 Height coordinate

Separation metric in pressure coordinate is useful since observation data and reanalysis data are usually reported on pressure levels. However, it is limited due to the hydrostatic assumption. Current NWP models are capable of modeling nonhydrostatic flows, and a lot of predictability studies are conducted based on NWP modeling results (Zhang et al., 2007; Hohenegger and Schar, 2007; Qin and Mu, 2012). Therefore, the separation metric in height coordinate could be useful, which is not dependent on the hydrostatic assumption.

In height coordinate, the sum of kinetic energy, internal energy and geopotential energy

$$E=\int_A\int_{z_{\mathrm{H}}}^{\infty}\left(\frac{1}{2}\rho\boldsymbol{v}^2+\rho c_vT+\rho gz\right)\mathrm{d}z\mathrm{d}A, \tag{21}$$

is conserved (Vallis, 2006), where ρ is the density, $\boldsymbol{v}=(u,v,w)$ are velocities in the two horizontal and vertical directions in height coordinate, c_v is the specific heat for dry air at constant volume, z_{H} is the surface elevation, and the other symbols follow the same notation as Sect. 3. For an ideal gas, Eq. (21) can be rewritten as

$$E=\int_A\int_{z_{\mathrm{H}}}^{\infty}\left(\frac{1}{2}\rho\boldsymbol{v}^2+\frac{c_v}{R}p+\rho gz\right)\mathrm{d}z\mathrm{d}A. \tag{22}$$

ACPD
14, 3733–3775, 2014



By defining phase vector as $\boldsymbol{x} = (\sqrt{\rho}u, \sqrt{\rho}v, \sqrt{\rho}w, \sqrt{p}, \sqrt{\rho})$, Eq. (22) is the Euclidean norm. Hence, the separation metric of two vectors $\boldsymbol{x}_1$ and $\boldsymbol{x}_2$ is given by

$$\|\boldsymbol{x}_1 - \boldsymbol{x}_2\|^2 = \int_A \int_{z_H}^{\infty} \left(\frac{1}{2}(\delta\sqrt{\rho}\boldsymbol{v})^2 + \frac{c_v}{R}(\delta\sqrt{p})^2 + gz(\delta\sqrt{\rho})^2 \right) \mathrm{d}z\mathrm{d}A. \tag{23}$$

Actually, Eq. (23) is not dependent on the form of conserved energy. The separation metric induced by Eq. (21) is the same as that induced by Eq. (23). Compared to the separation metric in pressure coordinate, Eq. (23) has another density dimension $\sqrt{\rho}$. Note that the absence of a boundary-layer term in Eq. (23) is because the vertical coordinate of the bottom surface, i.e. surface elevation, is fixed in height coordinate.

Equation (23) can be linearized and approximated by conventional perturbations δu, δv, δw, δp and $\delta\rho$ as below

$$\|\boldsymbol{x}_1 - \boldsymbol{x}_2\|^2 \approx \int_A \int_{z_H}^{\infty} \left(\frac{1}{2} \left(\rho(\delta\boldsymbol{v})^2 + \boldsymbol{v}\cdot\delta\boldsymbol{v}\,\delta\rho + \frac{\boldsymbol{v}^2}{4\rho}(\delta\rho)^2 \right) + \frac{c_v}{R}\frac{(\delta p)^2}{4p} + gz\frac{(\delta\rho)^2}{4\rho} \right) \mathrm{d}z\mathrm{d}A, \tag{24}$$

The linear approximation requires the perturbation terms δu, δv, δw, δp and $\delta\rho$ to be much smaller than the variables u, v, w, p and ρ. There are mixed terms in the linearized metric similar to the shallow-water model. Equation (24) can be further simplified to

$$\|\boldsymbol{x}_1 - \boldsymbol{x}_2\|^2 \approx \int_A \int_{z_H}^{\infty} \left(\frac{1}{2}\rho(\delta\boldsymbol{v})^2 + \frac{c_v}{R}\frac{(\delta p)^2}{4p} + gz\frac{(\delta\rho)^2}{4\rho} \right) \mathrm{d}z\mathrm{d}A, \tag{25}$$

if $|\delta\boldsymbol{v}|/|\boldsymbol{v}| \gg |\delta\rho|/\rho$ holds true over most of the integration domain.

ACPD
14, 3733–3775, 2014



3.4 Generalized vertical coordinate

In Sects. 3.1 to 3.3, the upper boundary is always assumed to be at infinity. But in numerical model, it is impossible to cover the whole atmosphere hence an finite upper boundary is needed. Both the lower and upper boundaries are assumed to be material surfaces to conserve mass.

It has been shown (Kasahara, 1974; Staniforth and Wood, 2003) that energy in generalized vertical coordinate s

$$E = \int_A \int_{s_H}^{s_T} ((u^2 + v^2 + \delta_v w^2)/2 + c_v T + \Phi)\sigma_s \mathrm{d}s\mathrm{d}A, \tag{26}$$

is conserved only if the upper boundary is a rigid lid, i.e., z = constant, where $\sigma_s = \rho\partial z/\partial s$, Φ is the geopotential, δ_v is the switch between nonhydrostatic ($\delta_v = 1$) and hydrostatic ($\delta_v = 0$) equation, the subscripts H and T mean values at the lower and upper boundaries respectively, and the other symbols follow the same notation as in the previous sections. The integrand is similar to that in height coordinate except the density is multiplied by the Jacobian of the vertical coordinate transformation. No work is done at the upper boundary. For elastic lid, i.e. nonzero constant pressure at the upper boundary, an energy-like invariant (Staniforth et al., 2003)

$$E = \int_A \int_{s_H}^{s_T} ((u^2 + v^2 + \delta_v w^2)/2 + c_v T + \Phi + p_T/\rho)\sigma_s \mathrm{d}s\mathrm{d}A, \tag{27}$$

exists. Work is done at the upper boundary, which incurs one more term in the energy expression.

Note that σ_s could be positive or negative depending on the definition of vertical coordinate s. For convenience, let the integration lower bound be $s_L = \min(s_H, s_T)$ and the

ACPD
14, 3733–3775, 2014



integration upper bound be $s_U = \max(s_H, s_T)$. If the two integral limits s_L and s_U are constant with time, then Eqs. (26) and (27) are Euclidean norms and the separation metrics are defined as in height coordinate. Otherwise, we need to define appropriate reference lower and upper bounds $s_{Lr}(x,y) \geq \sup_t\{s_L(x,y,t)\}$ and $s_{Ur}(x,y) \leq \inf_t\{s_U(x,y,t)\}$ and separate the atmosphere into a main body and boundary layers at the top and bottom to get the approximated energy norm, based on which the separation metric can be induced.

In the case of elastic lid, Eq. (27) can be rewritten as

$$E = \int_A \int_{s_L}^{s_U} (|\sigma_s|(u^2 + v^2 + \delta_v w^2)/2 + c_v|\sigma_s|T + |\sigma_s|\Phi + p_T|J|)\mathrm{d}s\mathrm{d}A, \tag{28}$$

where $J = \partial z/\partial s$ is the Jacobian of the vertical coordinate transformation. Like in the pressure and isentropic coordinates, Eq. (28) can be approximated by

$$\begin{aligned} E \approx & \int_A \int_{s_{Lr}}^{s_{Ur}} (|\sigma_s|(u^2 + v^2 + \delta_v w^2)/2 + c_v|\sigma_s|T + |\sigma_s|\Phi + p_T|J|)\mathrm{d}s\mathrm{d}A \\ & + \int_A (c_v|\sigma_s|_{Lr}T_{Lr} + |\sigma_s|_{Lr}\Phi_{Lr} + p_T|J|_{Lr})(s_{Lr} - s_L)\mathrm{d}A \\ & + \int_A (c_v|\sigma_s|_{Ur}T_{Ur} + |\sigma_s|_{Ur}\Phi_{Ur} + p_T|J|_{Ur})(s_U - s_{Ur})\mathrm{d}A, \end{aligned} \tag{29}$$

where $|\sigma_s|_{Lr}$, T_{Lr}, Φ_{Lr}, $|J|_{Lr}$ are the lower-boundary climatology and $|\sigma_s|_{Ur}$, T_{Ur}, Φ_{Ur}, $|J|_{Ur}$ are the upper-boundary climatology defined similarly as Eq. (18). Therefore the phase vector is defined as

$$\boldsymbol{x} = \left(\sqrt{|\sigma_s|}u, \sqrt{|\sigma_s|}v, \sqrt{|\sigma_s|}w, \sqrt{|\sigma_s|T}, \sqrt{|\sigma_s|\Phi}, \sqrt{|J|}, \sqrt{s_{Lr} - s_L}, \sqrt{s_U - s_{Ur}}\right),$$

ACPD
14, 3733–3775, 2014



and the separation metric based on Eq. (29) can be defined as before. The phase vector has a Jacobian dimension $\sqrt{|J|}$ due to the work done at upper boundary and two boundary-layer dimensions.

For a hydrostatic atmosphere, the energy-like invariant Eq. (28) can be simplified by combining internal energy, geopotential and the pressure work term (Staniforth et al., 2003) as

$$E = \int_A \int_{s_L}^{s_U} (\boldsymbol{u}^2/2 + c_p T + \Phi_H)|\sigma_s| \mathrm{d}s \mathrm{d}A. \tag{30}$$

Notice that the energy density in Eq. (30) reproduces the energy density in pressure and isentropic coordinates with infinite upper boundary. Hence in the case of a finite upper boundary with constant pressure, the separation metric Eq. (14) is also valid but integrated up to a nonzero constant pressure instead of zero pressure.

4 Example I: geostrophic balanced flow of shallow-water model

In this section, the separation metric of shallow-water model is applied to an axisymmetric geostrophically balanced flow in polar coordinates. Let r and λ be the radial and angular coordinates respectively, $\boldsymbol{u} = (u, v)$, u and v be the radial and azimuthal velocity components, and the other symbols follow the same notation as previous sections. The flow is initially at rest with height given by

$$h_\circ = \begin{cases} -h'_\circ + H_\circ & r < a_1 \\ H_\circ & r > a_1, \end{cases} \tag{31}$$

ACPD
14, 3733–3775, 2014



where $H_\circ$ is the basic depth and $h'_\circ$ is the initial disturbance. The initial potential vorticity profile is

$$\mathrm{PV} = \frac{\zeta + f}{h} = \begin{cases} \frac{f}{-h'_\circ + H_\circ} & r < a_1 \\ \frac{f}{H_\circ} & r > a_1, \end{cases} \tag{32}$$

where $\zeta = r^{-1}\partial(rv)/\partial r$ is the relative vorticity. The geostrophic balanced state can be solved analytically by potential vorticity (PV) conservation without assumption of $h'_\circ \ll H_\circ$ as pointed by Mak (2011), where he gave the non-dimensional solution of geostrophic adjustment in Cartesian coordinates. The boundary conditions are: $\partial h/\partial r = 0$ at $r = 0$ and $h = 0$ as $r \to \infty$, which means the azimuthal velocity at the origin is zero and the perturbation dies away at infinity.

For simplicity, the following non-dimensional variables are introduced

$$\widetilde{h} = \frac{h}{H_\circ} = 1 + \widetilde{h'}, \widetilde{r} = \frac{r}{L_\mathrm{d}}, \widetilde{v} = \frac{v}{fL_\mathrm{d}}, \widetilde{\mathrm{PV}} = \frac{\mathrm{PV}}{f/H_\circ}, \widetilde{E} = \frac{E}{gH_\circ^2 L d^2}, \tag{33}$$

where $\widetilde{h'}$ is the non-dimensional perturbation height and $L_\mathrm{d} = \sqrt{gH_\circ}/f$ is the Rossby radius of deformation. Since the initial disturbance could be strong, it is necessary to consider the advection of fluid columns from initial positions (Mak, 2011). Let a_2 be the new PV discontinuity point, i.e. $a_2 - a_1$ is the displacement of the PV boundary. Then the non-dimensional conservation of PV becomes

$$\frac{\frac{\partial^2 \widetilde{h'}}{\partial \widetilde{r}^2} + \frac{1}{\widetilde{r}}\frac{\partial \widetilde{h'}}{\partial \widetilde{r}} + 1}{\widetilde{h'} + 1} = \begin{cases} 1/\eta & \widetilde{r} < a_2/L_\mathrm{d} \\ 1 & \widetilde{r} > a_2/L_\mathrm{d}, \end{cases} \tag{34}$$

where $\eta = -h'_\circ/H_\circ + 1$. The solution is determined by parameters $h'_\circ/H_\circ$ and a_2/L_d.

ACPD
14, 3733–3775, 2014



Solving Eq. (34) separately for $\widetilde{r} < a_2/L_d$ and $\widetilde{r} > a_2/L_d$ and matching the solutions at $\widetilde{r} = a_2/L_d$ gives the balanced perturbation height

$$\widetilde{h}' = \begin{cases} -\frac{h'_\circ}{H_\circ} + \frac{h'_\circ}{H_\circ}\frac{I_0(\widetilde{r}/\sqrt{\eta})}{M(a_2/L_d)} & \widetilde{r} \le a_2/L_d \\ -\frac{h'_\circ}{H_\circ}\frac{K_0(\widetilde{r})}{N(a_2/L_d)} & \widetilde{r} > a_2/L_d, \end{cases} \tag{35}$$

where I_α and K_α are the modified Bessel functions of the first kind and second kind,

$$M(x) = I_0(x/\sqrt{\eta}) + \frac{1}{\sqrt{\eta}}\frac{K_0(x)}{K_1(x)} I_1(x/\sqrt{\eta}), \tag{36}$$

and

$$N(x) = K_0(x) + \sqrt{\eta}\frac{I_0(x/\sqrt{\eta})}{I_1(x/\sqrt{\eta})} K_1(x). \tag{37}$$

The balanced velocity can be obtained

$$\widetilde{v} = \begin{cases} \frac{1}{\sqrt{\eta}}\frac{h'_\circ}{H_\circ}\frac{I_1(\widetilde{r}/\sqrt{\eta})}{M(a_2/L_d)} & \widetilde{r} \le a_2/L_d \\ \frac{h'_\circ}{H_\circ}\frac{K_1(\widetilde{r})}{N(a_2/L_d)} & \widetilde{r} > a_2/L_d, \end{cases} \quad \widetilde{u} = 0, \tag{38}$$

where a_2 is determined by the mass conservation equation

$$\int_0^\infty \widetilde{h}'\widetilde{r}\,d\widetilde{r} = \int_0^{a_1/L_d} (-h'_\circ/H_\circ\widetilde{r})\mathrm{d}\widetilde{r}. \tag{39}$$

The left hand side of Eq. (39) is a monotonic function of a_2, hence the solution of a_2 is unique and increases as a_1 increases.

ACPD
14, 3733–3775, 2014



The non-dimensional separation metric of two vectors $\widetilde{\boldsymbol{x}}_1$ and $\widetilde{\boldsymbol{x}}_2$ in polar coordinates is given by

$$\|\widetilde{\boldsymbol{x}}_1 - \widetilde{\boldsymbol{x}}_2\|^2 = \frac{1}{2}\int_0^\infty \left(\left(\delta\sqrt{\widetilde{h}\widetilde{v}} \right)^2 + (\delta\widetilde{h})^2 \right) \widetilde{r}\mathrm{d}\widetilde{r}. \tag{40}$$

Linearization of Eq. (40) gives

$$\|\widetilde{\boldsymbol{x}}_1 - \widetilde{\boldsymbol{x}}_2\|^2 \approx \frac{1}{2}\int_0^\infty \left(\widetilde{h}(\delta\widetilde{v})^2 + \frac{\widetilde{v}^2}{4\widetilde{h}}(\delta\widetilde{h})^2 + \widetilde{v}\delta\widetilde{v}\delta\widetilde{h} + (\delta\widetilde{h})^2 \right) \widetilde{r}\mathrm{d}\widetilde{r}, \tag{41}$$

where the integral of the first three terms are called kinetic separation.

The non-dimensional PV profile is shown in Fig. 1a with $a_1/L_\mathrm{d} = 4$ and $h'_\circ/H_\circ = 0.8$. Figure 1b and c shows the non-dimensional solutions of height and tangential velocity. The PV boundary is displaced from $\widetilde{r} = 4$ to $\widetilde{r} = 3.53$. The low-PV water mass originally at region D now moves to B and C and pushes the high-PV water mass originally at C to A. The tangential velocity maximizes at the new PV boundary a_2. The Rossby number $R_\circ = V/fL = \widetilde{v}L_\mathrm{d}/a_2$ is about 0.17 which is small so that the geostrophic approximation is good.

In order to investigate the importance of the mixed term in the separation metric, two sets of balanced solutions with different initial height discontinuity but the same initial radius of high PV ($a_1/L_\mathrm{d} = 4$) are investigated. The first case is $h'_\circ/H_\circ = 0.1$, where the flow is more like a linear system. The second case is $h'_\circ/H_\circ = 0.8$, where the flow is nonlinear. Separation metrics are calculated by adding perturbations to the two control parameters a_1/L_d and $h'_\circ/H_\circ$ for both cases. All perturbations are sufficiently small that linearization of the separation metric is good. The ratio between the mixed term $\frac{1}{2}\int_0^\infty (\widetilde{v}\delta\widetilde{v}\delta\widetilde{h})\widetilde{r}\mathrm{d}\widetilde{r}$ and the other two quadratic terms of the linearized kinetic separation for both cases are shown in Fig. 2. In the first case, the mixed term is always less than 5% of the first quadratic term. Hence in more linear flows, the non-Euclidean

ACPD
14, 3733–3775, 2014



separation metric can be approximated by ignoring the mixed terms. But in the second case, the amplitude of the mixed term could be comparable to the first quadratic term unless the perturbations are almost entirely in a_1/L_d. Essentially, in nonlinear flows, the non-Euclidean characteristic of the linearized separation metric cannot be neglected.

The nonlinear kinetic separation as in the first term of Eq. (40) for the second case where $h'_\circ/H_\circ = 0.8$ is shown in Fig. 3a. Note the range of perturbations on a_1/L_d and $h'_\circ/H_\circ$ are comparable to the parameters themselves. The linearized separation metric is only valid within a small region centered at the origin as shown by the large errors arising elsewhere if the linearized expression is used instead of the nonlinear expression (Fig. 3b).

5 Example II: 2-D thermal wind model in pressure coordinate

In this section, the separation metric of dry compressible atmosphere in pressure coordinate is applied to a 2-D thermal wind model. The zonal wind at surface is assumed be to zero. Potential temperature in radiative equilibrium is assumed to be

$$\frac{\theta}{\theta_\circ} = 1 - \Delta_h \sin^{\frac{8}{3}}\phi \frac{2\exp\{(p-p_{ch})/\Delta_p\} - 1}{2\exp\{(p-p_{ch})/\Delta_p\} + 1} + \Delta_v \ln\frac{p_H}{p}, \tag{42}$$

where ϕ is latitude with negative denoting the South Hemisphere, p_H is the surface pressure which is a constant in this simple model, $\theta_\circ$ is the surface temperature at equator, Δ_h and Δ_v control the fractional change of potential temperature from equator to pole and from the surface to the tropopause respectively, p_{ch} controls the pressure where equator-pole temperature difference changes sign, Δ_p is a factor controlling the vertical extent of the balanced jet and the other symbols follow the same notation as the previous sections. The form of Eq. (42) is inspired by the work of Held and Hou (1980).

ACPD
14, 3733–3775, 2014



It is convenient to introduce the following non-dimensional variables:

$$\widetilde{T} = \frac{T}{\theta_\circ}, \widetilde{u} = \frac{u}{R\theta_\circ/\Omega_e a}, \widetilde{p} = \frac{p}{p_H}, \widetilde{E} = \frac{E}{c_p \theta_\circ p_H a/g}, \tag{43}$$

where Ω_e is the angular speed of rotation of Earth, a is the radius of Earth, and the rest symbols follow the same notation as Sect. 3. So the non-dimensional thermal wind equation can be written as

$$2\sin\phi \frac{\partial \widetilde{u}}{\partial \widetilde{p}} = \frac{1}{\widetilde{p}} \frac{\partial \widetilde{T}}{\partial \phi}. \tag{44}$$

Given the equilibrium potential temperature, the non-dimensional temperature is

$$\widetilde{T} = \widetilde{p}^{R/c_p} \left(1 - \Delta_h \sin^{\frac{8}{3}}\phi \frac{2\exp\{(\widetilde{p} - \widetilde{p}_{ch})/\Delta_{\widetilde{p}}\} - 1}{2\exp\{(\widetilde{p} - \widetilde{p}_{ch})/\Delta_{\widetilde{p}}\} + 1} - \Delta_v \ln \widetilde{p}\right), \tag{45}$$

and the solution of zonal wind is obtained by integrating the right hand side of Eq. (44) from surface to $\widetilde{p}$. The non-dimensional separation metric is given by

$$\|\widetilde{\boldsymbol{x}}_1 - \widetilde{\boldsymbol{x}}_2\|^2 = \int_{-\frac{\pi}{2}}^{\frac{\pi}{2}} \int_0^1 \left(\frac{R^2\theta_\circ}{c_p \Omega_e^2 a^2} \frac{(\delta\widetilde{u})^2}{2} + \left(\delta\sqrt{\widetilde{T}}\right)^2 \right) \cos\phi \mathrm{d}\widetilde{p}\mathrm{d}\phi, \tag{46}$$

where we have used the fact that the depth of the atmosphere is much smaller than the radius of Earth. Notice that $\widetilde{T}$ and $\widetilde{u}$ are both well-defined finite function of $\widetilde{p}$ over [0, 1] so the integration is finite.

The following parameters are fixed: $\theta_\circ = 300\,\mathrm{K}$, $p_H = 1000\,\mathrm{mb}$, $p_{ch} = 220\,\mathrm{mb}$, $\Delta_v = 35/300$. We consider a reference solution with $\Delta_h = 40/300$ and $\Delta_{\widetilde{p}} = 50/1000$. Figure 4a and b shows the balanced temperature and zonal wind profiles of the reference solution in the Northern Hemisphere. The Southern and Northern Hemispheres

ACPD
14, 3733–3775, 2014



are symmetric. The westerly jet is formed around 40° N with the maximum velocity 21.5 m s^{-1} at about 200 mb. The thermal wind balance model is more valid in the mid-latitudes and hence the solution in the tropics is not a good approximation of the real atmosphere. Another deficiency is the vertical temperature profile in this model does not describe the temperature inversion above tropopause. Therefore we shall only make use of the data below 100 mb and between 35–65° N.

Separation metrics are calculated when Δ_h and $\Delta_{\tilde{p}}$ are perturbed. Figure 4c shows the non-dimensional kinetic and enthalpy components of the separation and the ratio between them. The kinetic component is found to be always less than the enthalpy component though the ratio between them varies with perturbations. The order of magnitude of the ratio kinetic to enthalpy components is set by the ratio of the potential temperature and specific angular momentum parameters, $\theta_\circ/(\Omega_e a)^2$ in the Earth's atmosphere. In the next section, the relative importance of kinetic and enthalpy components of separation is further investigated with reanalysis data.

6 Example III: reanalysis data of the atmosphere

The separation metric of a dry compressible atmosphere in pressure coordinate is also applied to the reanalysis data. The data used in this study is NCEP Climate Forecast System Reanalysis (CFSR) monthly mean of 6 hourly forecasts (CFSR, 2010). The reanalysis monthly mean data covers 31 yr from January 1979 to December 2009 with $0.5^\circ \times 0.5^\circ$ spatial resolution and 37 vertical levels from 1000 mb to 1 mb. Temperature, u- and v-component of wind at 37 pressure levels as well as surface geopotential height, pressure and temperature are needed for the calculation. The separation metric Eq. (15) is transformed from Cartesian coordinates to spherical coordinates with the Jacobian $r^2 \cos\phi$. Since the depth of the atmosphere is much smaller than the radius of Earth, the Jacobian can be approximated by $a^2 \cos\phi$.

Before applying, it is necessary to test the assumption that $[T(x,y,p,t)]_{[p_r,p_H]}$ does not vary much temporally. The results show its temporal perturbation is less than 2.5 %

ACPD
14, 3733–3775, 2014



of its climatology T_r globally. So the separation metric in Eq. (14) on pressure coordinate can be applied to both tropical and mid-latitude regions. It is also verify that the linearized separation metric in Eq. (15) is valid for use. Unless otherwise stated, the separation metric is summed over all pressure levels.

Separation metrics between CFSR monthly mean data and its annual mean climatology and seasonal climatology are both investigated. Here annual mean climatology is defined as the mean over all months in 31 yr, and so is time-independent. And seasonal climatology is defined as the mean over a certain calendar month, e.g. all the Januaries in 31 yr, and so is month-dependent. Separation from the former can be used to identify atmospheric oscillations, e.g. annual cycle and quasi-biennial oscillation (QBO) while separation from the latter is useful to identify inter-annual variations, e.g. the Southern Annular Mode (SAM).

6.1 Annual and interannual oscillations

The separation metric between CFSR monthly mean data and its annual mean climatology in the tropical region (25° S–25° N) up to 100 mb is calculated and the results between 2001 and 2009 are shown in Fig. 5a. Kinetic, enthalpy and surface pressure separations all show a synchronous semi-annual oscillation, which maximizes at January or February and July or August. This is consistent with the seasonal cycle: the atmosphere state moves further from the annual mean state during winter and summer. The kinetic separation is about one order of magnitude larger than the enthalpy separation. This can be explained by the near constancy of temperature and surface pressure and higher variation of velocity, e.g. the seasonal oscillation, in the tropical region.

The annual oscillation is further illustrated in Fig. 5b, which shows the time-latitude cross section of total separation integrated zonally and vertically in the tropical region. Contributions from the higher tropical latitudes are an order of magnitude larger than from the equatorial latitudes, which attests to the equitable climate near the equator.

ACPD
14, 3733–3775, 2014



The seasonality is stronger in the Northern Hemisphere compared to the same latitude in the Southern Hemisphere.

The QBO, a phenomenon observed in the mean zonal wind of the equatorial stratosphere, has an influence on the global stratosphere through modulation of winds, temperature and the meridional circulation (Baldwin et al., 2001). The meridional distribution of the amplitude of the QBO is approximately Gaussian, centered at the equator with a 12° half-width (Wallace, 1973). The separation metric between CFSR monthly mean data and its annual mean climatology in the equatorial tropics (5° S–5° N) integrated over the whole atmosphere column is calculated and shown in Fig. 6a. Further investigation of the separation metric level by level shows that on average, the kinetic and enthalpy separations in stratosphere (70 mb to 1 mb) contribute 39.3 % and 47.3 % respectively to the kinetic and enthalpy separations in the whole column (not shown). Although the QBO in wind is associated with a signature in temperature as well, the column integrated enthalpy separation consists of stronger seasonal variations than the kinetic separation does. Hence the temperature QBO signal is not identifiable in the column integrated enthalpy separation with the analysis methodology we used in this study. Only the analysis of the kinetic separation is presented below.

Since the kinetic separation also contains significant contribution from ENSO and seasonal variations, we first decompose the kinetic separation into the trend, oscillations and a residue using the singular-spectrum analysis (SSA). Between 1979 and 2009, 372 sample points are used. The window length is 36 sample points, i.e. 3 yr. RC(1) is the trend and explains 90.8 % of the total variance. The dominant oscillation is semi-annual and is captured by the 2nd and 3rd reconstructed components denoted by the RC(2, 3) explaining 3.5 % of the total variance. The RC(4, 5) shows the quasi-biennial oscillation explaining 1.4 % of the total variance. In order to confirm its relation with the QBO, RC(4, 5) is lag correlated with the absolute value of QBO index, which is defined as the zonal wind at 30 mb over Singapore. As shown in Fig. 6c, the maximum correlation score 0.54 is attained when the RC(4, 5) lags behind the QBO index by 5 months and the correlation score peaks every 28 months which is the average period

ACPD
14, 3733–3775, 2014



of the QBO. The RC(4, 5) shifted backward by 5 months matches the QBO index very well as shown in Fig. 6b, including years when the QBO period is longer than average, e.g. 1999 to 2002.

The lag correlation of the absolute value of QBO index with the kinetic separation at different pressure levels is shown in Fig. 6d. The correlation score maximizes at 30 mb with zero lag simply because the QBO index is defined at this level. Since the QBO phase propagates downward, the kinetic separation leads the QBO index at higher pressure levels than 30 mb and lags behind at pressures lower than 30 mb. Only the tilted positive correlation band centered at zero lag is physical. The other tilted correlation bands located at about multiples of 7 months away are just mirrored images produced by the quasi-periodicity of the QBO. The correlation score drops rapidly at 100 mb and pressure levels below (except around 500 mb), and becomes insignificant at the 99 % confidence level. We assume that the number of independent samples is 124, which is the number of seasons in our time series, giving the number of degrees of freedom as 122. For a monthly time series, there is likely some dependence between adjacent months. This is why we assume the size of independent sample to be the number of seasons instead of months.

There is some indication that QBO has a significant but weak influence in the mid-troposphere. A possible reason is that the zonal mean wind in the stratosphere modifies the vertical propagation of waves, leaving certain waves and their associated energy trapped in the troposphere. The influence of QBO in troposphere is better captured by our energy metric than by the physical variables themselves probably because our metric is related directly to the total energy norm.

6.2 Thermal wind

To compare with the 2-D thermal wind model in Sect. 5, the separation metric between zonal mean CFSR monthly mean data and its annual mean climatology in midlatitudes (35–65° N) up to 100 mb is calculated and the results between 2001 and 2009 are shown in Fig. 7a. For the locations where the pressure level is below the surface, data

ACPD
14, 3733–3775, 2014



there are not included when taking the zonal mean. Kinetic and enthalpy components show a synchronous semi-annual oscillation as in the tropics. The surface pressure component is noisier and the semi-annual oscillation is not obvious. The reason is that surface pressure has stronger zonal asymmetry due to the distribution of continents and major oceans. The seasonal cycles of surface pressure of continents and oceans at the same latitude are not in phase. Hence the zonal mean surface pressure is not a good indicator of the seasonal cycle.

A noticeable difference from the tropics is that the kinetic component is smaller than the enthalpy component, which agrees with the results in the analytical thermal wind model. The ratio of kinetic component over enthalpy component is about 0.42 on average. The larger separation in enthalpy results from the strong seasonal variation of temperature in midlatitudes.

It has been shown in the Lorenz energy cycle (Holton, 2004) that baroclinic eddies are the primary driving force for the energy exchange in midlatitudes. However, the importance of eddies has been neglected in the calculation above with zonal mean data. To reveal the contribution to the separation metric from eddies, the same separation metric calculated from full 3-D data including the eddies is shown in Fig. 7b. The kinetic separation is found to be comparable to the enthalpy separation. The difference between the two separation metrics (based on zonal mean data and 3-D data) is considered to be contributed by the eddies. On average, eddies contribute 78 % to the total kinetic separation and 27 % to the total enthalpy separation. The contribution from the eddies to the separation metric is in good agreement with the contribution from eddies to energy in Lorenz energy cycle, where eddies contribute 71 % to the total kinetic energy and 31.8 % to the total available potential energy (Oort and Peixóto, 1974). This is probably because we are using an energy-norm induced metric.

In Sect. 3.1, we have seen that the coefficient of temperature difference $(\delta T)^2/T$ in our separation metric is different from the coefficient of temperature T in the total energy norm Eq. (1). The same enthalpy separation metric as in Fig. 7b is calculated but using slightly modified formulae. Figure 7c shows the effects of using constant temper-

ACPD
14, 3733–3775, 2014



ature $T_\circ = 270\,\mathrm{K}$ in the enthalpy separation $c_p(\delta T)^2/(4T_\circ)$, multiplying a factor of two $c_p(\delta T)^2/(2T_\circ)$ and choosing $p_\mathrm{r} = 1000\,\mathrm{mb}$. Note the coefficient $c_p/(2T_\circ)$ in the second modified formula is the one commonly used in the literature (Ehrendorfer and Errico, 1995; Errico, 2000; Qin and Mu, 2012). It is found that using constant temperature $T_\circ = 270\,\mathrm{K}$ instead of the realistic reference temperature does not change the enthalpy separation much. But the factor of two does make the contribution from the enthalpy separation more significant.

6.3 Southern Annular Mode

The Southern Annular Mode (SAM) refers to the alternating pattern of stronger and weaker westerlies together with negative and positive pressure anomalies between the mid to high latitudes in the Southern Hemisphere. It is the leading mode of variability of the Southern Hemisphere climate (Thompson and Wallace, 2000). A review of various SAM definitions and indices can be found in Ho et al. (2012). In this study, we adopt the Gong and Wang (1999) definition of SAM index given by

$$\text{SAM index} = P^*_{40^\circ\mathrm{S}} - P^*_{65^\circ\mathrm{S}},$$

where $P^*_{40^\circ\mathrm{S}}$ and $P^*_{65^\circ\mathrm{S}}$ is the normalized zonal mean sea level pressure for every month at 40° S and 65° S respectively. The index is calculated using CFSR monthly mean data.

Separation metric between CFSR monthly mean data and its seasonal climatology within 35–65° S is calculated and shown in Fig. 8. The kinetic and surface pressure separations are of the same order and a few times larger than the enthalpy separation. We have illustrated the difference between our proposed separation metric and the total energy norm in Eq. (1) for the enthalpy component in Sect. 6.2. Apart from that, coefficients for surface pressure perturbations are quite different. With the total energy norm Eq. (1) divided by a constant g, the surface pressure separation from that formula is smaller by a factor between 17.6 and 18.6 than that from our formula but the variation pattern would be preserved as shown in Fig. 8. This is mainly because we

ACPD
14, 3733–3775, 2014



divide the surface pressure perturbation by boundary-layer mass instead of the whole atmospheric column mass, as is reasonable in a metric based on the energy norm. Therefore, the total energy norm Eq. (1) overestimates the enthalpy separation and underestimates the surface pressure separation compared to our proposed separation metric.

The reference pressure p_r in the separation metric Eq. (14) is location-dependent, which would result in a different horizontal distribution of surface pressure separation and hence total separation compared to that calculated with the total energy norm Eq. (1) where the surface pressure contribution is negligible. Figure 9 compares the horizontal distribution of column integrated total separation metric on July 1992 with that calculated with the total energy norm Eq. (1). As is shown, features A and B in Fig. 9a have different patterns from those in Fig. 9b.

To show the separation metric carries the signal of SAM, it is correlated with the absolute value of SAM index. The correlation score of absolute value of SAM index with surface pressure separation attains the maximum value 0.35 at zero lag, which is significant at the 99% level (assuming the number of independent samples is 124, which is the number of seasons of our time series, giving the number of degrees of freedom as 122).

7 Conclusions

A new approach to define the separation metric is proposed to give a quantitative measure of how different two atmospheric states are. The atmospheric phase vector is defined such that the square root of energy is the Euclidean norm in the phase space and the square of the norm induced metric is referred as the separation metric. The separation metric can be applied to both linear and nonlinear flows.

The separation metric is first derived for the 2-D barotropic model, in which energy is the Euclidean norm in the phase space formed by the horizontal wind. In the subsequent shallow-water model, a new unconventional phase vector is defined

ACPD
14, 3733–3775, 2014



as $\boldsymbol{x} = (\sqrt{h}u, \sqrt{h}v, h)$ so that energy norm is Euclidean. Although the transformation from this energy-proper coordinates $(\sqrt{h}u, \sqrt{h}v, h)$ to the more conventional coordinates (u, v, h) is nonlinear, the Euclidean separation metric in the energy-proper coordinates is linearly approximated in the conventional coordinates. The linearized separation metric in the conventional coordinates is non-Euclidean, which is applied to an analytical model of a geostrophically balanced flow. The model results illustrate that in highly nonlinear systems, the non-Euclidean terms of the linearized separation metric cannot be neglected.

The separation metric is also derived for the 3-D compressible model in various vertical coordinates including pressure, isentropic, height and the generalized vertical coordinate. The separation metric in pressure coordinate is applied to a 2-D thermal wind model and Climate Forecast System Reanalysis (CFSR) data. It is found that the separation metric is able to capture seasonal (Fig. 5) and interannual oscillations (Figs. 6 and 8) and exhibit the dynamics of thermal wind balance and Lorenz energy cycle.

Compared to our proposed separation metric, we find that the total energy norm in the literature has doubled the contribution from the enthalpy separation (Fig. 7c). In addition, it underestimates the surface pressure separation by one order of magnitude (Fig. 8a). Such a big quantitative difference arises from our understanding of the role of the surface pressure term: it represents the mass fluctuations in the surface boundary layer and hence the denominator in the term has $p_{\mathrm{H}} - p_{\mathrm{r}}$ in Eq. (15) instead of $p_{\circ}$ in Eq. (1).

The separation metric is a useful measure of the difference between two atmospheric states. We suggest that the formulation of our metric is rigorous and physically meaningful, hence we recommend its use in practice. For example, it can also be a choice for the cost function in data assimilation, which quantifies the deviations of the analysis values from the observations (Kalnay, 2003). However, the separation metrics in this study are developed for dry models. we are working next on the separation metric including moisture and applying it to real cases.

ACPD
14, 3733–3775, 2014



Appendix A

Choice of p_r

The reference pressure $p_r < \inf_t\{p_H(x,y,t)\}$ is subject to two constraints. On one hand, it should be close to p_H so that surface pressure component represents the fluctuations in a boundary layer. On the other hand p_r should be chosen so that the surface pressure component in Eq. (14), i.e. $(\delta\sqrt{p_H - p_r})^2$, is not sensitive to the perturbation of p_r. Let's define

$$f(p_{H1}, p_{H2}, p_r) = (\sqrt{p_{H1} - p_r} - \sqrt{p_{H2} - p_r})^2. \quad \text{(A1)}$$

The surface pressure variation is of the order 10 mb hence without loss of generality, let $p_{H2} = p_{H1} + 10$ mb hence f is a function of $p_{H1} - p_r$. For a given value of p_{H1} and p_r, the sensitivity of f to the perturbation Δp_r in p_r can be illustrated by the the percentage change

$$|f(p_{H1} - p_r - \Delta p_r) - f(p_{H1} - p_r)|/f(p_{H1} - p_r). \quad \text{(A2)}$$

For a decrease of 10 mb in p_r, the percentage change depends only on the thickness of the boundary layer $p_{H1} - p_r$, which is shown in Fig. A1. The sensitivity increases exponentially as the boundary layer thickness approaches zero. Considering both constraints, the boundary layer thickness of 100 mb is reasonable as the percentage change of f is lower than 10 %.

Acknowledgements. We would like to thank the examiners of the first author's PhD thesis and their valuable comments.

References

Baldwin, M. P., Gray, L. J., Dunkerton, T. J., Hamilton, K., Haynes, P. H., Randel, W. J., Holton, J. R., Alexander, M. J., Hirota, I., Horinouchi, T., Jones, D. B. A., Kinnersley, J. S.,

ACPD
14, 3733–3775, 2014



Marquardt, C., Sato, K., and Takahashi, M.: The quasi-biennial oscillation, Rev. Geophys., 39, 179–229, 2001. 3756
Bannon, P. R.: Hydrostatic adjustment: Lamb's problem, J. Atmos. Sci., 52, 1743–1752, 1995. 3735
Buizza, R., Tribbia, J., Molteni, F., and Palmer, T.: Computation of optimal unstable structures for a numerical weather prediction model, Tellus A, 45, 388–407, 1993. 3735, 3737
CFSR: Environmental Modeling Center/National Centers for Environmental Prediction/National Weather Service/NOAA/US Department of Commerce, NCEP Climate Forecast System Reanalysis (CFSR) Monthly Products, January 1979 to December 2010, Research Data Archive at the National Center for Atmospheric Research, Computational and Information Systems Laboratory, available at:http://rda.ucar.edu/datasets/ds093.2 (last access: 15 May 2013), 2010. 3754
Davidson, K. R. and Donsig, A. P.: Real analysis and applications theory in practice, Undergraduate Texts in Mathematics, Springer, 2010 Edn., New York, 2010. 3736
Ding, R. and Li, J.: Nonlinear finite-time Lyapunov exponent and predictability, Phys. Lett. A, 364, 396–400, 2007. 3735
Ehrendorfer, M. and Errico, R. M.: Mesoscale predictability and the spectrum of optimal perturbations, J. Atmos. Sci., 52, 3475–3500, 1995. 3735, 3737, 3759
Errico, R. M.: Interpretations of the total energy and rotational energy norms applied to determination of singular vectors, Q. J. Roy. Meteor. Soc., 126, 1581–1599, 2000. 3735, 3759
Fleisch, D.: A Student's Guide to Vectors and Tensors, 1st Edn., Cambridge University Press, New York, 2011. 3739
Gong, D. and Wang, S.: Definition of Antarctic oscillation index, Geophys. Res. Lett., 26, 459–462, 1999. 3759
Held, I. M. and Hou, A. Y.: Nonlinear axially symmetric circulations in a nearly inviscid atmosphere, J. Atmos. Sci., 37, 515–533, 1980. 3752
Ho, M., Kiem, A. S., and Verdon-Kidd, D. C.: The Southern Annular Mode: a comparison of indices, Hydrol. Earth Syst. Sci., 16, 967–982, doi:10.5194/hess-16-967-2012, 2012. 3759
Hohenegger, C. and Schar, C.: Atmospheric predictability at synoptic versus cloud-resolving scales, B. Am. Meteorol. Soc., 88, 1783–1794, 2007. 3744
Holton, J. R.: An Introduction to Dynamic Meteorology, 4th edn., International Geophysics Series, Academic press, 2004. 3758

ACPD
14, 3733–3775, 2014



Kalnay, E.: Atmospheric Modeling, Data Assimilation, and Predictability, Cambridge University Press, Cambridge, 2003. 3761
Kasahara, A.: Various vertical coordinate systems used for numerical weather prediction, Mon. Weather Rev., 102, 509–522, 1974. 3746
Kim, H., Kim, S., and Jung, B.: Real-time adaptive observation guidance using singular vectors for typhoon Jangmi (200815) in T-PARC 2008, Weather Forecast., 26, 634–649, 2011. 3735
Leutbecher, M. and Palmer, T. N.: Ensemble forecasting, J. Comput. Phys., 227, 3515–3539, 2008. 3735, 3737
Lorenz, E. N.: Deterministic nonperiodic flow, J. Atmos. Sci., 20, 130–141, 1963. 3734
Lorenz, E. N.: A study of the predictability of a 28-variable atmospheric model, Tellus, 17, 321–333, 1965. 3734
Lorenz, E. N.: Predictability of a flow which possesses many scales of motion, Tellus, 21, 289–307, 1969. 3735, 3738
Mak, M.: Atmospheric Dynamics, 1st Edn., Cambridge University Press, New York, 2011. 3749
Molteni, F. and Palmer, T. N.: Predictability and finite-time instability of the northern winter circulation, Q. J. Roy. Meteor. Soc., 119, 269–298, 1993. 3735
Mu, M. and Duan, W.: A new approach to studying ENSO predictability: conditional nonlinear optimal perturbation, Chinese Sci. Bull., 48, 1045–1047, 2003. 3735
Mu, M., Duan, W., and Wang, B.: Conditional nonlinear optimal perturbation and its applications, Nonlinear Proc. Geoph., 10, 493–501, 2003. 3735
Oort, A. H., and Peixóto, J.: The annual cycle of the energetics of the atmosphere on a planetary scale, J. Geophys. Res., 79, 2705–2719, 1974. 3758
Palmer, T. N., Gelaro, R., Barkmeijer, J., and Buizza, R.: Singular vectors, metrics, and adaptive observations, J. Atmos. Sci., 55, 633–653, 1998. 3735, 3737
Qin, X. and Mu, M.: Influence of conditional nonlinear optimal perturbations sensitivity on typhoon track forecasts, Q. J. Roy. Meteor. Soc., 138, 185–197, 2012. 3735, 3744, 3759
Rivière, O., Lapeyre, G., and Talagrand, O.: A novel technique for nonlinear sensitivity analysis: application to moist predictability, Q. J. Roy. Meteor. Soc., 135, 1520–1537, 2009. 3735
Staniforth, A. and Wood, N.: The deep-atmosphere Euler equations in a generalized vertical coordinate, Mon. Weather Rev., 131, 1931–1938, 2003. 3742, 3746
Staniforth, A., Wood, N., and Girard, C.: Energy and energy-like invariants for deep non-hydrostatic atmospheres, Q. J. Roy. Meteor. Soc., 129, 3495–3499, 2003. 3746, 3748

ACPD
14, 3733–3775, 2014



Talagrand, O.: A study of the dynamics of four-dimensional data assimilation, Tellus, 33, 43–60, 1981. 3735
Thompson, D. W. J. and Wallace, J. M.: Annular modes in the extratropical circulation, Part I: month-to-month variability, J. Climate, 13, 1000–1016, 2000. 3759
Trenberth, K. E.: Using atmospheric budgets as a constraint on surface fluxes, J. Climate, 10, 2796–2809, 1997. 3740, 3742
Vallis, G. K.: Atmospheric and Oceanic Fluid Dynamics: Fundamentals and Large-Scale Circulation, Cambridge University Press, New York, 2006. 3738, 3744
Wallace, J. M.: General circulation of the tropical lower stratosphere, Rev. Geophys., 11, 191–222, 1973. 3756
Yoden, S.: Dynamical aspects of stratospheric vacillations in a highly truncated model, J. Atmos. Sci., 44, 3683–3695, 1987. 3734
Zhang, F., Snyder, C., and Rotunno, R.: Effects of moist convection on mesoscale predictability, J. Atmos. Sci., 60, 1173–1185, 2003. 3735
Zhang, F., Bei, N., Rotunno, R., Snyder, C., and Epifanio, C. C.: Mesoscale predictability of moist baroclinic waves: convection-permitting experiments and multistage error growth dynamics, J. Atmos. Sci., 64, 3579–3594, 2007. 3744
Zou, X., Vandenberghe, F., Pondeca, M., and Kuo, Y. H.: Introduction to adjoint techniques and the MM5 adjoint modeling system, NCAR Technical Note, Boulder, 1997. 3735

ACPD
14, 3733–3775, 2014



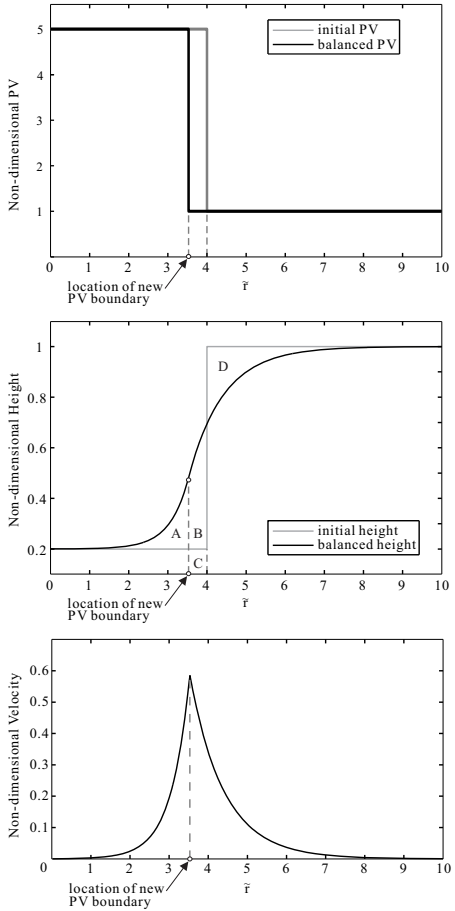


Fig. 1. Non-dimensional solution of PV, height and tangential velocity with $a_1/L_d = 4$ and $h'_o/H_o = 0.8$ in the geostrophic balanced shallow-water model.

ACPD
14, 3733–3775, 2014



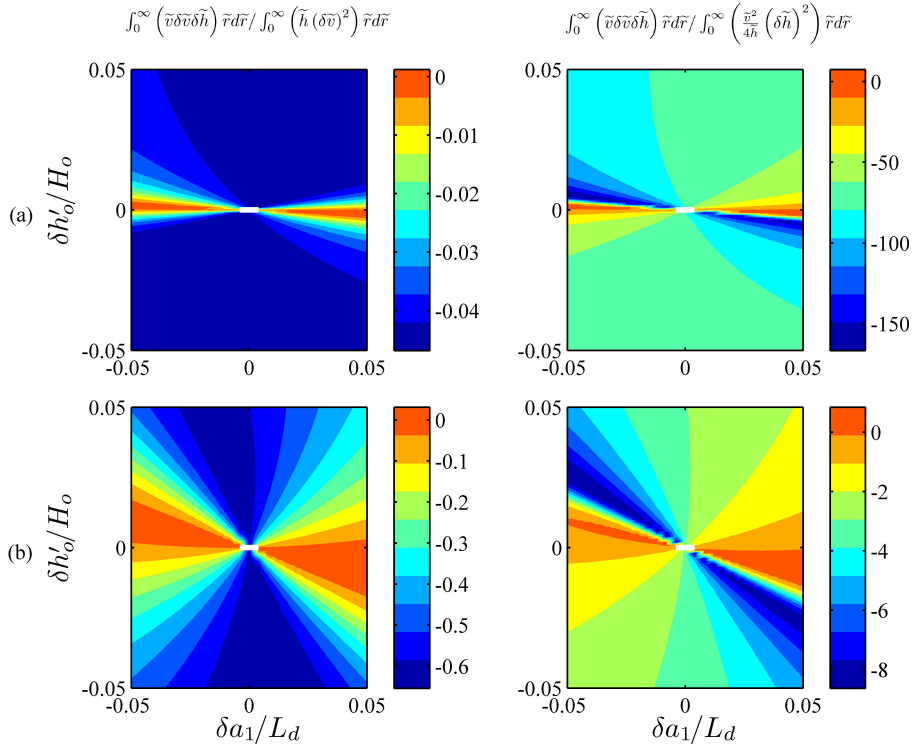


Fig. 2. The ratio between the mixed term and the other two quadratic terms of the linearized kinetic separation when $a_1/L_d = 4$ and **(a)** $h_o'/H_o = 0.1$ and **(b)** $h_o'/H_o = 0.8$. Value at the origin is not defined.

ACPD
14, 3733–3775, 2014



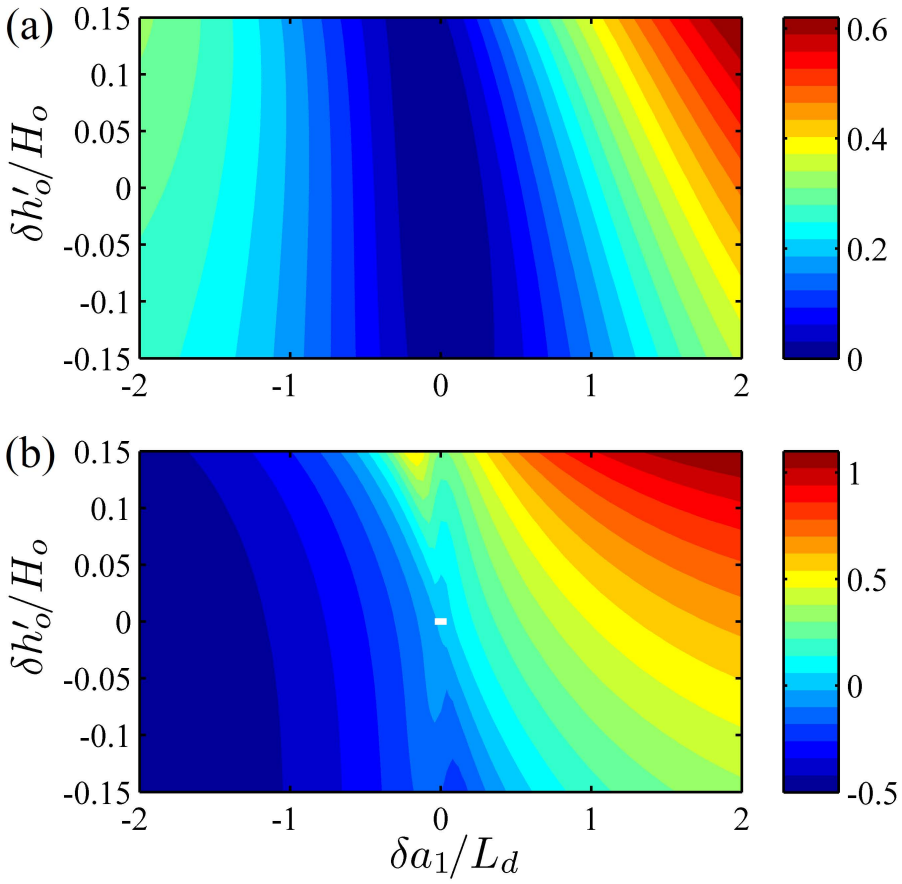


Fig. 3. (a) The non-dimensional kinetic separation (the first term of Eq. (42) when $a_1/L_d = 4$ and $h'_o/H_o = 0.8$. **(b)** Fractional error of linearized kinetic separation (the first three terms of Eq. (43) from **(a)**.

ACPD
14, 3733–3775, 2014



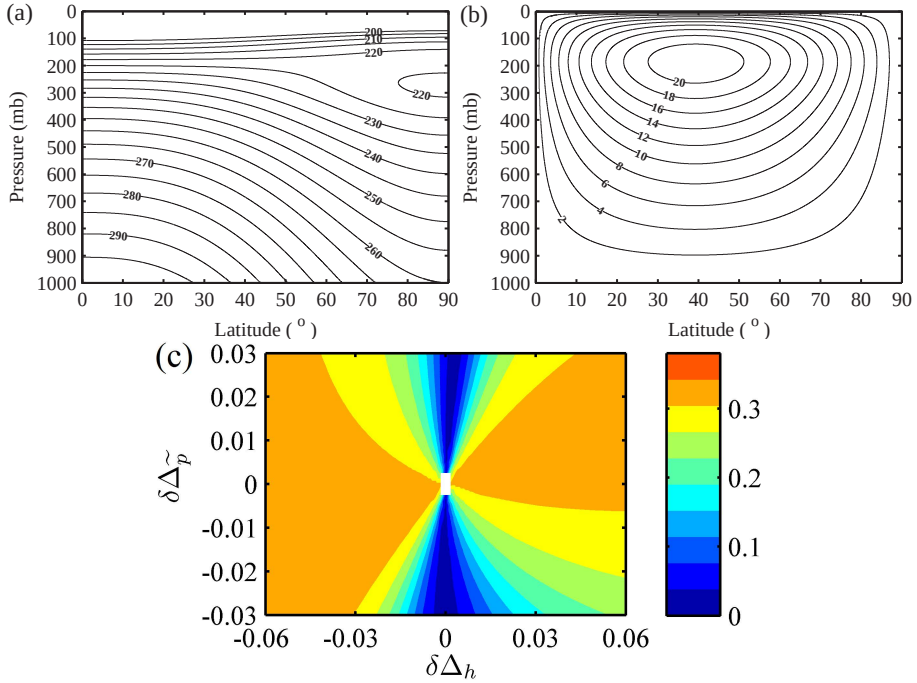


Fig. 4. (a) Balanced temperature and **(b)** zonal wind in the North Hemisphere of the 2-D thermal wind model. **(c)** Ratio between non-dimensional kinetic and enthalpy components of separation when Δ_h and $\Delta_{\tilde{p}}$ are perturbed.

ACPD
14, 3733–3775, 2014



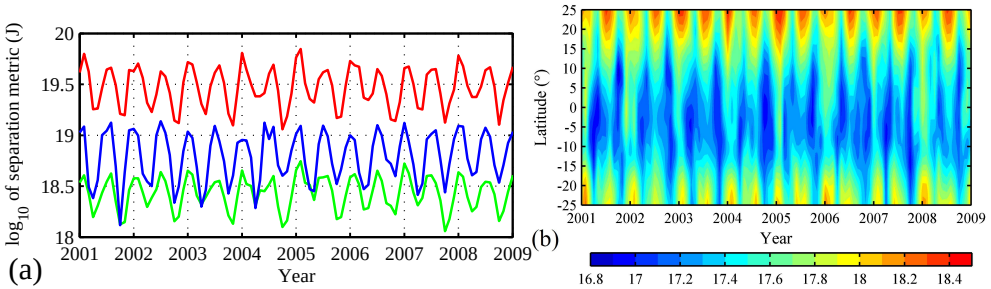


Fig. 5. (a) Kinetic (red), enthalpy (green) and surface pressure (blue) separations between CFSR monthly mean data and its annual mean climatology in the tropical region (25° S–25° N) up to 100 mb. **(b)** Time–latitude cross section of the logarithm to base 10 of the total separation integrated zonally and vertically up to 100 mb in the tropical region.

ACPD
14, 3733–3775, 2014



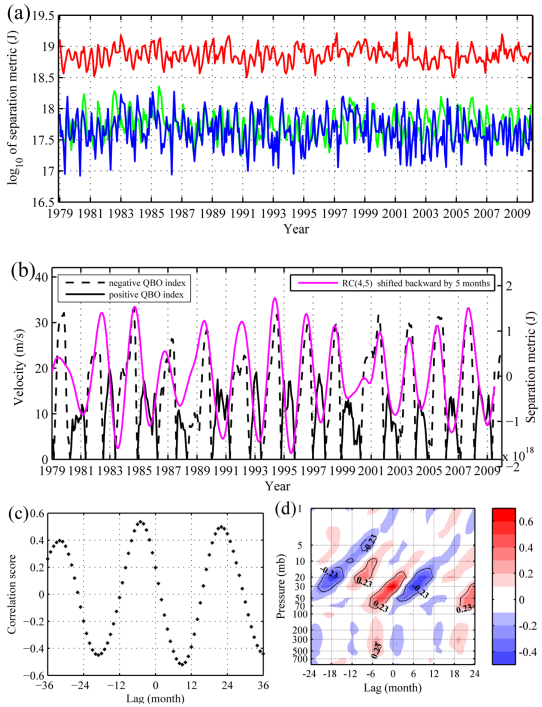


Fig. 6. (a) shows the kinetic (red), enthalpy (green) and surface pressure (blue) separations between CFSR monthly mean data and its annual mean climatology in the equatorial tropics (5° S–5° N) integrated over the whole atmosphere column. **(b)** shows the amplitude of the QBO index (black) and the RC(4, 5) of kinetic separation (magenta) shifted backward by 5 months. Black solid dash lines represent westerly and easterly zonal wind respectively. **(c)** Lag correlation of |QBO index| with the RC(4, 5) of kinetic separation. **(d)** Same as **(c)** but with the kinetic separation at different pressure levels. The black contour lines denote the 99% confidence level.

ACPD
14, 3733–3775, 2014



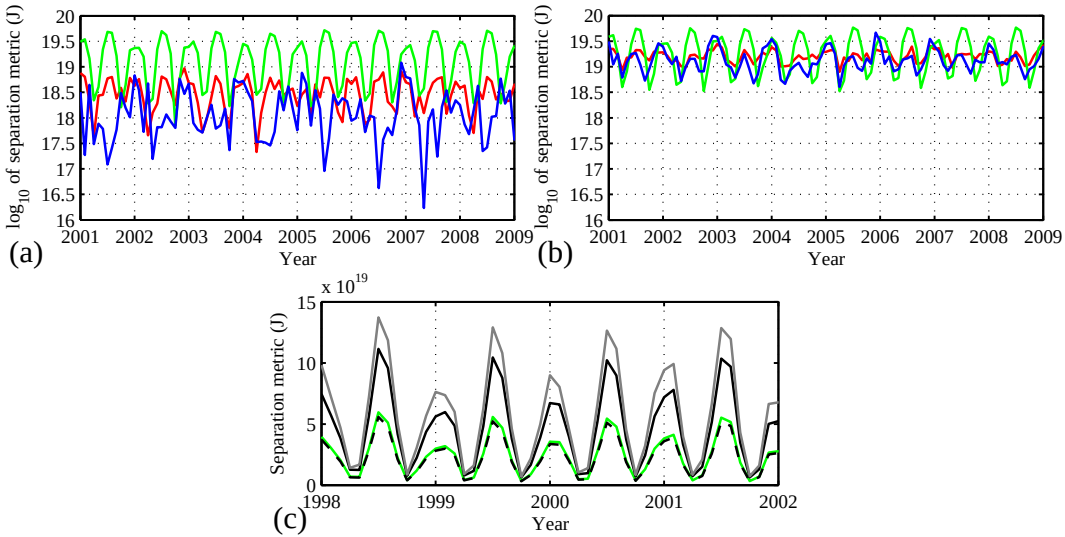


Fig. 7. (a) Kinetic (red), enthalpy (green) and surface pressure (blue) separations between zonal mean CFSR monthly mean data and its annual mean climatology in midlatitudes (35–65° N) up to 100 mb. **(b)** Same as **(a)** but using full 3-D data including the eddies. **(c)** Same as **(b)** but comparing only enthalpy components between 1998 and 2002 calculated with formulae: as the author proposed (green), using constant temperature $T_\circ$ = 270 K in the integrand $c_p(\delta T)^2/(4T_\circ)$ (black dash line), multiplying a factor of two $c_p(\delta T)^2/(2T_\circ)$ (black solid line) and choosing p_r = 1000 mb (gray). Note the logarithmic vertical scale in **(a)** to **(b)**.

ACPD
14, 3733–3775, 2014



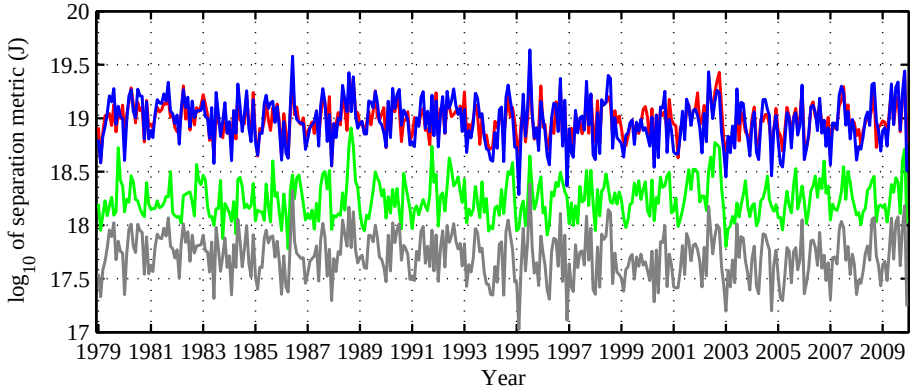


Fig. 8. Kinetic (red), enthalpy (green) and surface pressure (blue) separations between CFSR monthly mean data and its seasonal climatology in South Hemisphere mid-latitudes (35–65° S) integrated over the whole atmosphere column. Surface pressure component calculated with formula as Eq. (1) (gray).

ACPD
14, 3733–3775, 2014



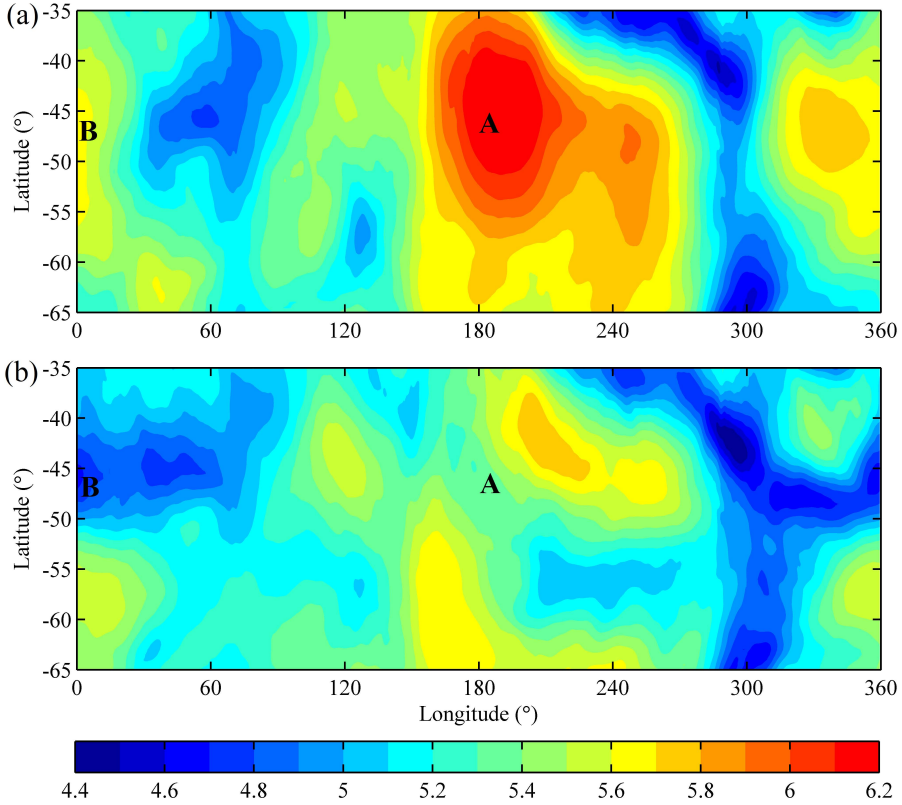


Fig. 9. (a) Horizontal distribution of $\log_{10}$ of column integrated total separation metric ($\mathrm{J\,m^{-2}}$) on July 1992. **(b)** Same as **(a)** but calculated with the total energy norm Eq. (1).

ACPD
14, 3733–3775, 2014



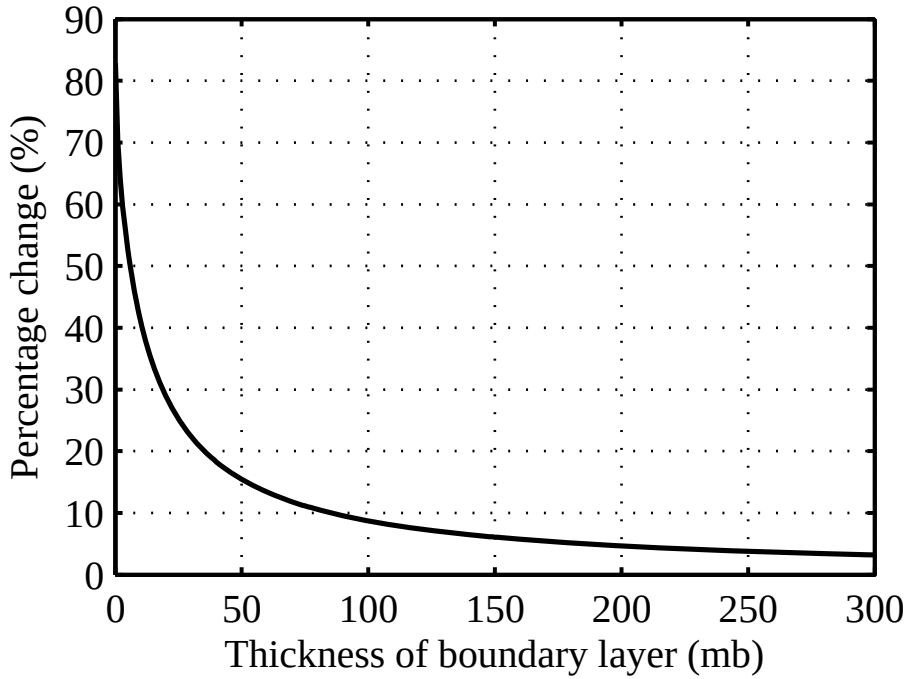


Fig. A1. Percentage change of the surface pressure separation due to a decrease of 10 mb in p_r as a function of boundary layer thickness $p_{H1} - p_r$.

ACPD
14, 3733–3775, 2014

